

Article

Real-Time Optimal Flow Setting and Respiratory Profile Evaluation in Infants Treated with High-Flow Nasal Cannula (HFNC) †

Francesco Montecchia ^{1,*}  and Paola Papoff ²

¹ Medical Engineering Laboratory, Department of Civil Engineering and Computer Science Engineering, University of Rome “Tor Vergata”, 1 Politecnico Street, 00133 Rome, Italy

² Pediatric Intensive Care Unit, Department of Pediatrics, Sapienza University of Rome, 00100 Rome, Italy; paola.papoff@uniroma1.it

* Correspondence: francesco.montecchia@uniroma2.it

† This paper is an extended version of the paper published in the Proceedings of IEEE MeMeA, Turin, Italy, 7–9 May 2015.

Abstract: High-flow nasal cannula (HFNC) is becoming the gold standard to treat respiratory distress at any age since it potentially provides several significant clinical advantages. An obstacle to the diffusion of this simple and effective system of oxygen therapy is the impossibility to know the optimal flow rate leading to such advantages that allows the reduction in the respiratory effort without causing hyperinflation. To assist clinicians during HFNC treatment in setting the optimal flow rate and in determining the most relevant parameters related to respiratory mechanics and the effort of the patient, we developed a new programmable data monitoring, acquisition, and elaborating system (Pro_HFNC). The application of Pro_HFNC is fully compatible with HFNC as it is interfaced with patient through a facial mask and two specific catheters. The unavoidable and unpredictable loss of air flow occurring around the contour of the mask is evaluated and compensated by a specific algorithm implemented by Pro_HFNC. Our preliminary clinical trials on pediatric patients treated with HFNC show that Pro_HFNC is actually capable to detect for any specific patient both the lower threshold of the delivered flow beyond which the benefits of HFNC application are reached and all the parameters useful for a complete evaluation of the respiratory profile. Pro_HFNC can really help physicians in setting the optimal flow rate during HFNC treatment, thus allowing for the most effective HFNC performance.

Keywords: respiratory system; respiratory flow; fluid dynamic model; computational modeling; patient-specific simulation; medical applications; medical devices; processing algorithm



Citation: Montecchia, F.; Papoff, P. Real-Time Optimal Flow Setting and Respiratory Profile Evaluation in Infants Treated with High-Flow Nasal Cannula (HFNC). *Fluids* **2024**, *9*, 93. <https://doi.org/10.3390/fluids9040093>

Academic Editors: Fang-Bao Tian and Xinguang Cui

Received: 16 February 2024

Revised: 5 April 2024

Accepted: 16 April 2024

Published: 18 April 2024



Copyright: © 2024 by the authors. Licensee MDPI, Basel, Switzerland. This article is an open access article distributed under the terms and conditions of the Creative Commons Attribution (CC BY) license (<https://creativecommons.org/licenses/by/4.0/>).

1. Introduction

Nasal cannulas (NCs) have been commonly used to deliver supplemental oxygen to patients with hypoxemic respiratory failure. Over the last twenty years, several studies have shown that if supplemental oxygen is delivered at high flow rate through NC, a positive distending pressure is generated in the oropharynx similarly to that provided using nasal continuous positive airway pressure (NCPAP) modalities. This new modality of delivering oxygen therapy is presently known as high-flow nasal cannula oxygen therapy (HFNC). HFNC delivers to patients a high flow of a warmed and humidified known air/oxygen mixture via NC, which exceeds the patient’s peak inspiratory flow (PIF). Thus, because the nasopharyngeal dead space is continuously purged by a high flow, the ratio of alveolar ventilation to minute ventilation increases, and a significant level of pharyngeal pressure is generated.

There are now several commercially available systems which combine the use of HFNC systems with a variety of different methods to condition breathing gases, high-flow oxygen being cold and dry and poorly tolerated [1].

The application of positive distending pressure at oropharynx via HFNC is an attractive option to intensive care physicians because of its relative ease of use, cost effectiveness, and patient tolerability [2,3]. Patients ranging in age from preterm newborns to adults receive flow rates from 2 to 60 L/min to support breathing through a variety of clinical conditions. For example, in neonatal practice, where respiratory illnesses are a major cause of morbidity and mortality, HFNC is often used as an alternative to NCPAP. In addition, HFNC devices are increasingly being used for a range of applications in pediatric patients with respiratory distress from infectious causes, such as viral bronchiolitis or bacterial pneumonia, to reactive airway diseases that might have otherwise required intubation or more uncomfortable techniques of non-invasive ventilation [4]. In adults, HFNC is used in a variety of clinical settings where increased flow rates are believed to benefit the patient, such as pulmonary edema, chronic obstructive pulmonary disease, or respiratory distress post-extubation.

In conventional NCPAP therapy, the patient breathes from a pressurized circuit, in which the pressure is controlled via an expiratory valve. Contrarily to NCPAP, with HFNC devices, the entire flow is continuously directed through the NC into the nasopharynx. In this case, the only flow escape routes are the leaks around the NC and via the mouth. In addition, there is no control device for delivery pressure. Therefore, if NC fits snugly into the patient's nose, and the mouth is closed, the pharyngeal pressure (P_{ph}) will depend entirely on the HFNC flow values. HFNC could thereby inadvertently generate dangerously high levels of P_{ph} that may lead to excessive lung overexpansion and worsening respiratory distress [5]. Therefore, the flow setting and systematic control of the P_{ph} are of critical importance to avoid excessively high intrathoracic pressures. Optimal flow setting is also important to satisfy the patient's flow requirement during inspiration. This point is crucial for the performance of HFNC. In fact, while using HFNC, when the inspired gas flow exceeds the patient's PIF, the nasopharyngeal cavity is continuously purged during the entire respiratory cycle. This purging of anatomical dead space removes expiratory gas that is high in CO₂ and relatively depleted of O₂ and creates an anatomical reservoir of the delivered air/oxygen mixture. Under these conditions, during subsequent breaths the patient will rebreathe less CO₂ and more O₂. The new alveolar gas equilibrium supports alveolar ventilation with higher alveolar partial pressure of oxygen (PaO₂) and lower alveolar partial pressure of carbon dioxide (PaCO₂). In addition, if the gas flow inspired through the NC exceeds the patient's PIF there will be no entry of air from the environment and the concentration of inspired oxygen would be the same as the one set on the HFNC blender, known as fraction of inspired oxygen (FiO₂) [1,4].

Although HFNC was developed as a procedure with no monitoring requirement, today's expanded use requires extended physiologic studies to guide clinicians in setting HFNC flow rate [6–10].

The effectiveness of HFNC depends on flow setting, which is frequently determined by the patient's weight at a rate of 1 to 2 L/min/kg. However, this empirical method may not be accurate and could result in treatment failure. To ensure accuracy, PIF should be measured before initiating HFNC. However, even with this information, it would be unknown what effects HFNC therapy has on patients' PIF, and whether the set HFNC flow becomes inadequate or excessively high after HFNC begins. Thus, we wondered whether evaluating PIF only once before HFNC therapy and then using this PIF value to set HFNC without further verification would be the right way to match patients and HFNC flow. An empirically consistent scenario is that PIF will change once HFNC therapy begins. Indeed, breathing frequency slows during HFNC, and longer times flatten the flow tracings, thus reducing PIF. Equally important, because HFNC therapy reduces esophageal pressure swings, PIF values will likely diminish. Thus, after HFNC starts, reduced PIF values might meet at different HFNC flow rate thresholds.

For this purpose, based on our previous experience [11], we specifically designed a new programmable data monitoring, acquisition, and elaboration system (Pro_HFNC) and tested its effectiveness on a series of young infants hospitalized in the Pediatric Intensive

Care Unit (PICU) at Sapienza University of Rome (Italy) with mild to moderate acute respiratory failure treated with HFNC.

2. Materials and Methods

In order to test the functional features of Pro_HFNC, we enrolled five infants less than 6 months of age with mild to moderate acute respiratory failure. The infants were studied once they were deemed stable by the clinical team and informed consent was obtained from the parents or guardians. The study was conducted in the 10-bed Pediatric Intensive Care Unit at Sapienza University of Rome’s Policlinico Umberto I teaching hospital. The study protocol received approval from the Policlinico Umberto I Review Board.

2.1. HFNC Delivery

To deliver HFNC (Fisher & Paikel Healthcare, Auckland, New Zealand), the infants were fitted with the appropriate-sized NC (Optiflow Junior NC, Fisher and Paykel, Auckland, New Zealand). Flow rate was set using a flow meter connected with a ventilation circuit (VC) (Optiflow Junior RT330, Fisher and Paykel, Auckland, New Zealand) which included a MR850 heater humidifier (Fisher and Paykel, Auckland, New Zealand) set at 37 °C. The outer diameter of NC did not exceed 80% of the infants’ nostril diameter to allow for adequate air leak.

2.2. Pph Monitoring

Pph was measured using a 6 Fr feeding catheter with 3 holes at the distal extremity. The catheter was inserted through the mouth in the pharynx (the tip just above the glottis) and connected to a differential pressure transducer (DPT) to measure Pph (DPT_4, Figure 1). To avoid occlusion of the catheter by secretions, a 20 mL/h airflow produced by a microinfusor was applied at the inlet of the catheter.

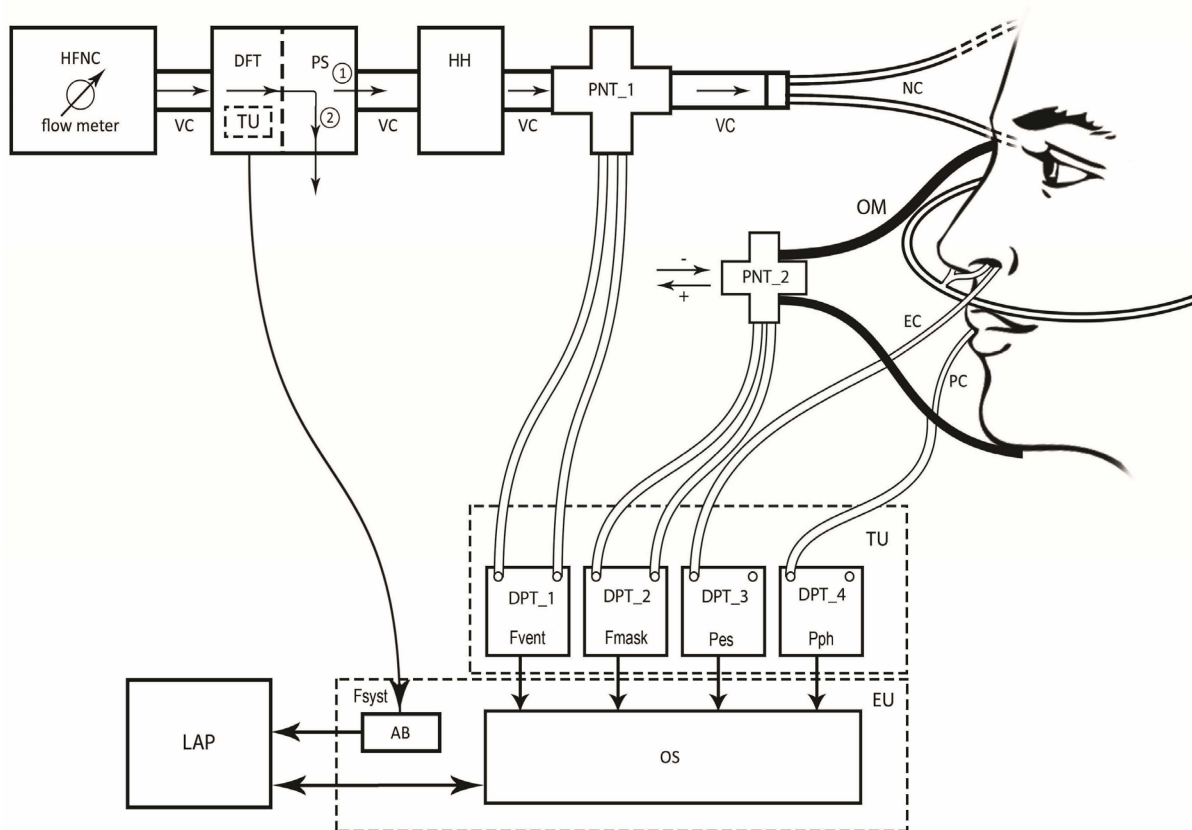


Figure 1. The Pro_HFNC setup showing high-flow nasal cannula (HFNC) flow meter, the ventilation circuit (VC), the digital flow transducer (DFT) coupled with a pneumatic switch (PS) and connected

to Arduino board (AB), the heater humidifier (HH) device, the first pneumotachograph (PNT_1) coupled with differential pressure transducer (DPT_1) and the nasal cannulas (NC) connected to the patient having an esophageal catheter (EC), and a pharyngeal catheter (PC) in place connected to the DPT_3 and DPT_4, respectively. The circled number 1 indicates that the patient is connected to the HFNC. The circled number 2 indicates that the patient has been disconnected from the HFNC. Placed on the patient's face is an oronasal mask (OM) on the main opening of which the second pneumotachograph (PNT_2) is inserted. The PNT_2 is coupled with DPT_2. The output signals from DPTs are connected to the respective input channels of an advanced oscilloscope (OS). The DFT and the four DPTs coupled with the four respective PNTs belonging to the Transducer Unit (TU), while AB and OS to the Electronic Unit (EU). Both OS and AB are then connected to a laptop computer (LAP) where the monitoring and elaboration software runs. F_{syst}: flow delivered by HFNC (without patient); F_{vent}: F_{syst} when the patient is connected to the HFNC; F_{mask}: flow intercepted by the OM; P_{es}: esophageal pressure; P_{ph}: pharyngeal pressure. As shown by the arrows, F_{vent} is always directed from HFNC flow meter to NC, while F_{mask} from the inside to the outside of the OM being considered as positive, or the vice versa being considered as negative.

2.3. Pes Monitoring

P_{es} was measured using an air-filled catheter with a thin-walled balloon over its distal end (AVEA smartcath esophageal pressure monitoring tube set 6 Fr pediatric, Carefusion, Yorba Linda, CA, USA). The balloon prevents occlusion of the catheter from fluid in the esophagus. When the volume of gas within the balloon is below its unstressed volume (i.e., its transmural pressure is zero), the pressure sensed within the balloon equals the pressure in the esophagus. Because the filled balloon will also distend the esophagus, keeping the gas volume to a minimum (typically 0.5 mL) will avoid producing a positive transmural pressure in the esophagus. The distal catheter segment contained within the balloon has 6 side-holes to assure continuity of gas flow between the balloon and catheter lumen. Balloons of approximately 5 cm in length offer stable measurements over a range of gas volumes and a firm position within the esophagus. The balloon catheter was firmly attached to a 6 Fr gauge catheter, which was connected to a DPT (DPT_3, Figure 1). The catheter was inserted through the nostril into the stomach (the position was checked by gentle manual pressure on the patient's abdomen to observe gastric pressure fluctuation). Then, the catheter was slowly pulled up until it remained in the middle portion of the esophagus. This position was confirmed by an oscillating signal with clear negative deflection simultaneous to inspiration on the monitor. In case of doubt, when a diagnostic chest X-ray film was performed on the infant, the balloon was left in place to confirm the position. The P_{es} measurement was validated by the dynamic occlusion test [12]. It consisted of measuring the ratio of change in P_{es} to that of airway pressure (P_{aw}) ($\Delta P_{es}/\Delta P_{aw}$ ratio) during three to five spontaneous respiratory efforts against a closed airway. An OM with a special material and shape, which allowed for a good pneumatic seal with no air leaking, whose opening could be blocked and whose internal pressure measured, was used for the purpose. The acceptable range of $\Delta P_{es}/\Delta P_{aw}$ ratio during the occlusion test was 10–20% (i.e., from 0.8 to 1.2). P_{aw} and P_{es} were recorded simultaneously.

2.4. Flow Detection

The flow delivered by HFNC without patient (F_{syst}) was measured using a digital flow transducer (DFT) inserted in series into the VC between the flow meter and the HH (Figures 1 and 2). To accurately detect F_{syst}, a pneumatic switch (PS) coupled with the DFT allowed for the temporary (less than 2 s) disconnection of the patient from VC (position 2), so as to avoid the interference of the patient's spontaneous respiratory activity on the F_{syst} signal. This maneuver was only required once at the beginning of the monitoring. The digital output of DFT was connected to the input of Arduino board (AB) for signal conversion (Figure 1).

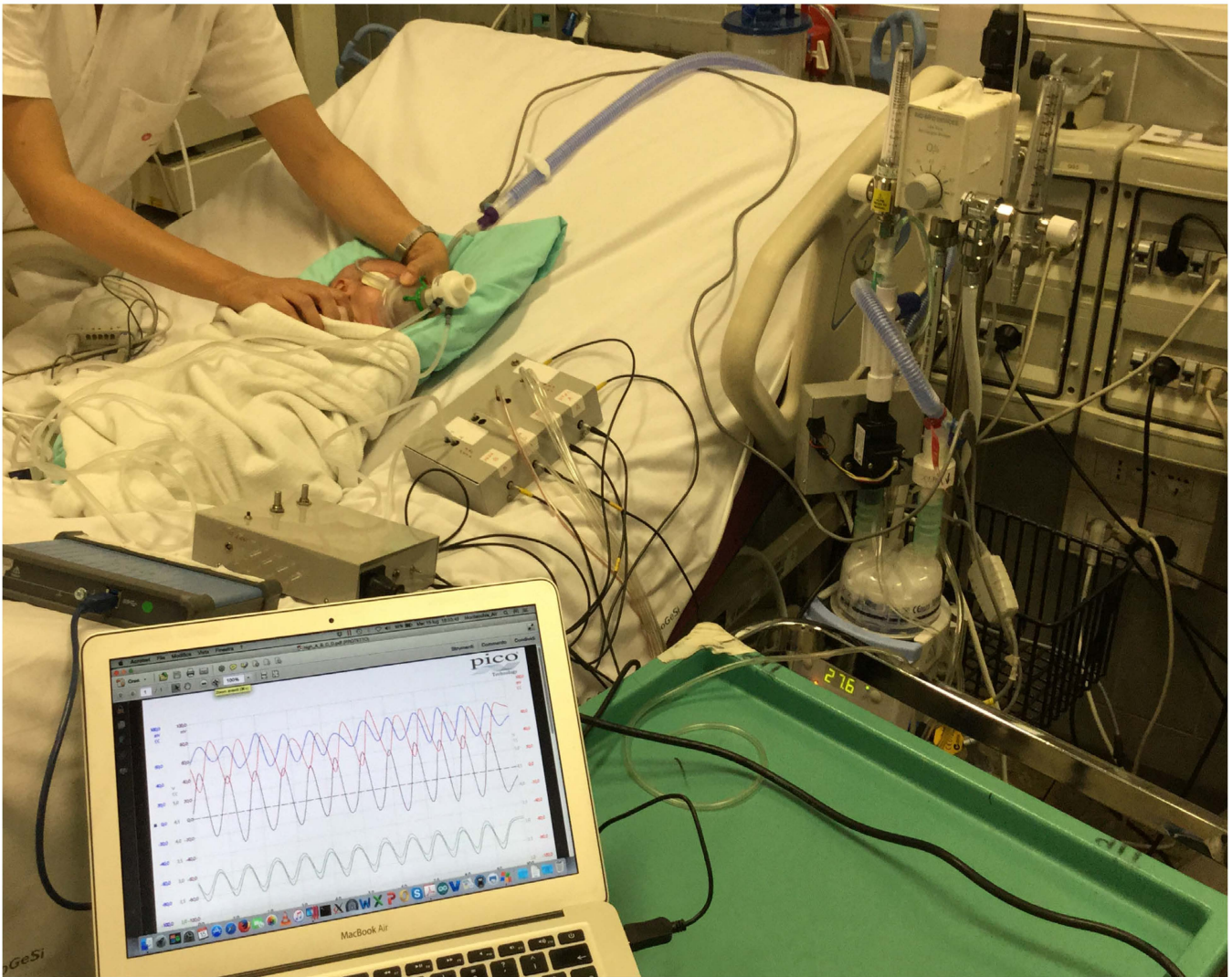


Figure 2. The picture shows the application of Pro_HFNC on a representative patient.

For advanced flow detection and optimal HFNC setting, two pneumotachographs (PNT: PNT_1 and PNT_2) were assembled in the Pro_HFNC (Figures 1–3). PNT_1 was inserted in the VC between the HH and the NC for online monitoring of the HFNC flow when the patient is connected to the HFNC (Fvent). PNT_2 was connected to the opening of an OM temporarily placed on the patient's face for online monitoring of the flow intercepted by the OM (Fmask). Both PNTs (PNT_1 and PNT_2) were coupled to the respective DPTs (DPT_1 and DPT_2) whose analogic outputs were connected to the respective input channels of an advanced oscilloscope (OS) (Figure 1).

2.5. Respiratory Flow and Tidal Volume Calculation

The respiratory flow (F_{resp}) waveform was calculated considering the model whose scheme is shown in Figure 3. The model incorporates the HFNC system and the VC, including the NC, the OM, and the patient.

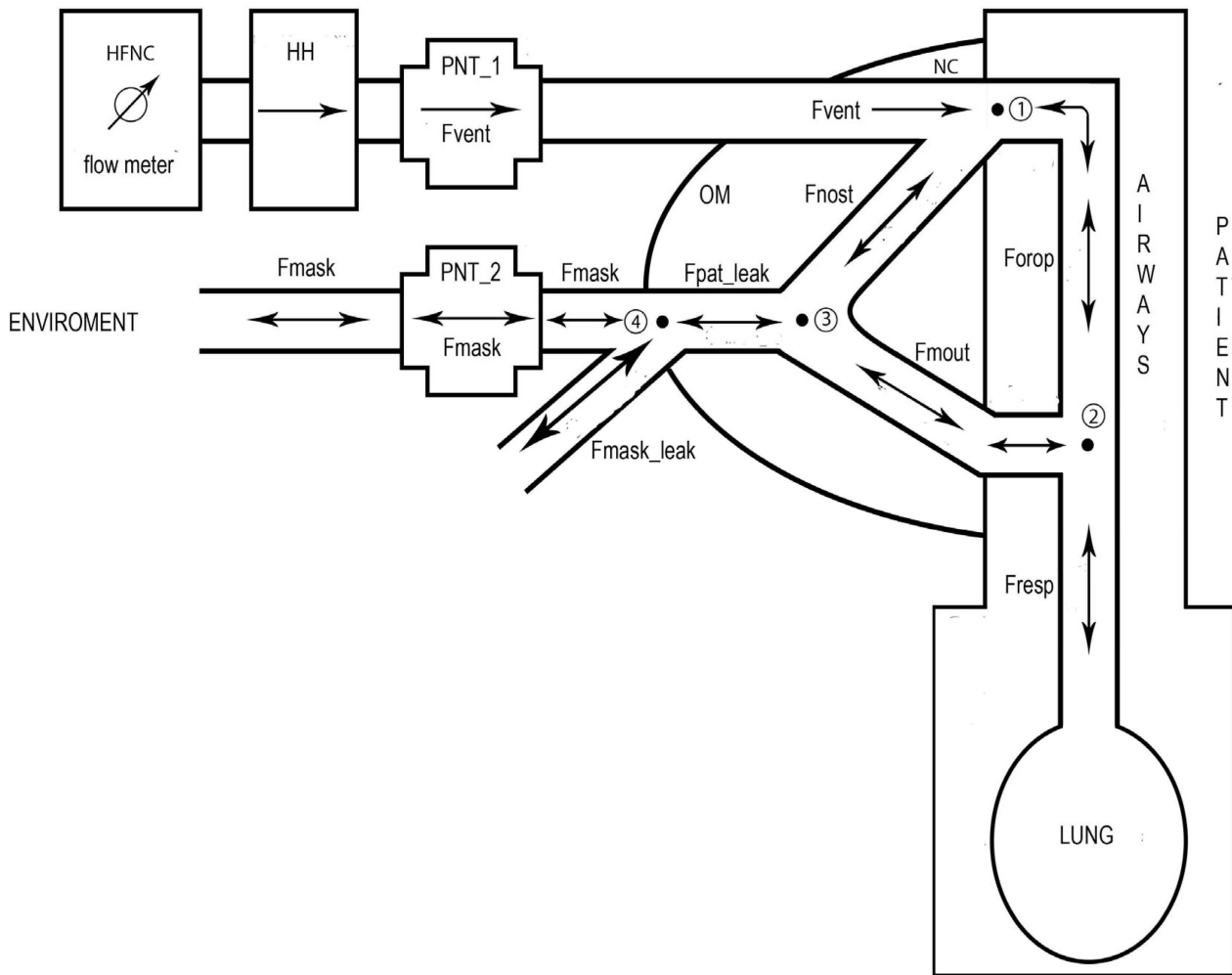


Figure 3. Schematic representation of the model employed to calculate the respiratory flow (F_{resp}). A first pneumotachograph (PNT_1) is inserted in the ventilation circuit to detect the flow delivered by the HFNC to the patient (F_{vent}). A second PNT_2 is inserted in the main opening of an oronasal mask (OM) to detect the flow intercepted by the OM (F_{mask}). The circled numbers 1,2,3 and 4 indicate the four nodes where the continuity law was applied. F_{nost} , F_{orop} , and F_{mout} are the flow around the nasal cannula (NC), the flow passing by the oropharynx, and the flow crossing the mouth, respectively. F_{pat_leak} is the sum of F_{nost} with F_{mout} which represents the difference between F_{vent} and F_{resp} . F_{pat_leak} is also the sum of F_{mask} with the flow leak along the OM edge (F_{mask_leak}). F_{mask_leak} is computed by the flow-based version of a specific algorithm [13]. In this figure are also shown the four nodes where the continuity law was applied (see Section 2.5: Equations (1), (2), (5), and (7)). The arrows indicate the direction of each specific flow which can be unidirectional (single arrows) or bidirectional (double arrow).

The arrows shown in Figure 3 indicate the direction of each specific flow which can be unidirectional (single arrow) or bidirectional (double arrow). Considering as positive flows those directed toward the node and as negative those directed outward the node, the application of the continuity law (currently Kirchoff’s law) to the nodes 1 and 2 gives the following equations:

$$F_{vent} = F_{nost} + F_{orop} \tag{1}$$

$$F_{orop} = F_{mout} + F_{resp} \tag{2}$$

where F_{nost} is the flow around the NC, F_{orop} is the flow passing by the oropharynx, and F_{mout} is the flow crossing the mouth. By inserting Equation (2) in Equation (1), the following equations can be obtained:

$$F_{vent} - F_{nost} = F_{mout} + F_{resp} \quad (3)$$

$$F_{resp} = F_{vent} - (F_{nost} + F_{mout}) \quad (4)$$

Applying the continuity law to the node 3, the following equation can be written:

$$F_{nost} + F_{mout} = F_{pat_leak} \quad (5)$$

where F_{pat_leak} is the total amount of air leak occurring at patient external airways. By inserting Equation (5) in Equation (4), the following equation can be obtained:

$$F_{resp} = F_{vent} - F_{pat_leak} \quad (6)$$

Applying the continuity law to the node 4, the following equation can be written:

$$F_{pat_leak} = F_{mask} + F_{mask_leak} \quad (7)$$

where F_{mask_leak} is the flow leak along the OM edge. Finally, by inserting Equation (7) in Equation (6) the following equation can be obtained:

$$F_{resp} = F_{vent} - F_{mask} - F_{mask_leak} \quad (8)$$

From Equation (8) it is clear that in order to compute the waveform of F_{resp} it is necessary to monitor the waveform of three flows, two of which, F_{vent} and F_{mask} , are directly available by PNT_1 and PNT_2, respectively. The third, i.e., F_{mask_leak} , was calculated by the flow-based version of a specific flow-leak correction algorithm, implemented online in the functional features of Pro_HFNC, which has already proven its effectiveness in advanced experimental test and in the clinical setting of HFNC [13]. Such version of the algorithm requires inputs from the monitoring of both F_{vent} and F_{mask} [13].

Once F_{resp} waveform was computed, the waveform associated with the change in inspiratory tidal volume (VT_i) was calculated by F_{resp} integration over inspiratory time.

2.6. Experimentals

2.6.1. Setup

The Pro_HFNC consisted of the following functional units (Figures 1 and 2): HFNC flow meter; DFT, which allowed for monitoring F_{syst} signal; HH; PNT_1, which allowed for monitoring F_{vent} signal; VC; OM; Transducer Unit (TU); Electronic Unit (EU); and laptop personal computer (LAP).

The Pro_HFNC was connected to the patient by esophageal (EC) and pharyngeal (PC) catheters for relative pressure measurements (P_{es} , P_{ph}), and by an OM equipped with PNT_2, which allowed for the monitoring of F_{mask} signal (Figures 1–3). Each patient studied was monitored by a cardiomonitor (Siemens, SC 9000 XL, Munich, Germany) for peripheral oxygen saturation (SpO_2), heart rate, and respiratory rate. Before connecting Pro_HFNC to the patient, HFNC was commenced empirically at 1 L/min/kg and increased to 2 L/min/kg by the attending physician according to blood gases and clinical signs of respiratory distress. After the patient was deemed stable, EC and PC were positioned (an IV bolus of 0.1 mg/kg midazolam was given to the patient to limit discomfort). Each catheter was connected to the TU (Figure 1). Baseline measurements were made during spontaneous breathing in low flow oxygen, then with HFNC. At each step, we respected a stabilization period of 10 min before any measurement. Recordings were made during a 5 min additional period. All recordings were performed in a semi-recumbent position.

2.6.2. Transducer Unit (TU)

The TU comprised a DFT, two PNTs, and an array of four DPTs, two of which were coupled with two PNTs, and the other two were connected with both EC and PC. The DFT is the Zephyr Digital HAF series – High Accuracy: full scale = 100 L/min (Honeywell, Charlotte, NC, USA). The PNTs are the PNT series 3700 not heated, Pediatrics flow range 0–160 L/min (Hans Rudolph, Shawnee, OK, USA). The DPTs coupled with the two PNTs are two SensorTechnics 144LU01D-PCB: full scale = ± 2.54 cmH₂O (SensorTechnics, Inc., Mansfield, CA, USA), whereas those coupled with EC and PC are two SensorTechnics 144LU10D-PCB: full scale = ± 25.4 cmH₂O.

2.6.3. Electronic Unit (EU)

The EU included two components: the PicoScope 4824 portable oscilloscope, Pico Technology, St Neots, UK (OS), and the Arduino Input/Output board (AB). The OS has several functions: (1) monitoring the DPTs output voltage signals, (2) converting them into the appropriate physical units, (3) filtering the signals, and (4) sampling and acquiring data for online and offline analysis and elaboration. The OS presents the following functional features: 8 independent input channels, 20 MHz bandwidth, 80 MS/s sampling rate, and 12-bit vertical resolution. The AB was used to convert the DFT digital output signal into the appropriate physical unit.

2.6.4. Laptop Personal Computer Unit (LAP)

The LAP supported an in-house-developed software to control AB, OS for the monitoring of all the signals, and the MATLAB (R2020a) platform employed for the analysis and the elaboration of all the monitored signals including the flow-based version of flow-leak correction algorithm [13].

2.7. Procedures

2.7.1. Measurements and Errors

In this work, all the data imported by MATLAB routines (Section 2.7.2) are relative to the following respiratory signals acquired by the AB or OS of TU (Figure 1):

- (1) F_{syst} , obtained from the DFT;
- (2) F_{vent} , obtained from the DPT_1 coupled with the PNT_1;
- (3) F_{mask} , obtained from the DPT_2 coupled with the PNT_2;
- (4) P_{es} , obtained from the DPT_3;
- (5) P_{ph} , obtained from the DPT_4.

Accuracy is the maximum deviation in output from nominal value over the entire calibrated flow/pressure range at 25 °C. Accuracy errors include offset, full-scale span, linearity, flow/pressure hysteresis, and repeatability. Total error includes accuracy errors, temperature span, and thermal hysteresis. The typical uncertainty (error) of measurement was 0.20 L/min (± 0.10 L/min) for F_{syst} , 0.25 L/min (± 0.13 L/min) for F_{vent} and F_{mask} , and 0.10 cmH₂O (± 0.05 cmH₂O) for P_{es} and P_{ph} . All these measurement errors are compatible with the accuracy and precision required for processing F_{syst} , F_{vent} , F_{mask} , P_{es} , and P_{ph} signals; for determining the optimal F_{vent} ; for the computation of the flow-based version of the correction algorithm; and for calculating all the parameters of the patient's respiratory profile.

Considering that the maximum expected breathing frequency is 120 acts per minute, corresponding to 2 Hz, the acquisition of the F_{vent} , F_{mask} , P_{es} , and P_{ph} signals was performed by setting OS with the following parameters:

- (1) A time window of 10 s;
- (2) A sampling rate of 1500 samples/s, producing a total number of 15,000;
- (3) A low pass filter, with a cut-off frequency of 5 Hz, to reject any kind of noise affecting the data.

The time window was selected in order to monitor about 10 respiratory cycles, while the sampling rate was selected in order to fit the scan speed of the time window with the maximum breathing frequency. As low pass filter, the OS uses a digital moving average filter for low cut-off frequencies. The OS adjusts the length of the filter to obtain the selected cut-off frequency, defined as the first minimum in the frequency response. There is a significant loss of signal above the cut-off frequency. This filter changes a front vertical descent into a linear one. This kind of filter does not introduce any artifact in the signals, so it does the selected cut-off frequency, which is considerably greater than the maximum expected breathing frequency.

2.7.2. MATLAB Routines

The ALGOLEAK routine implements the flow-based version of a proper and specific algorithm [13] that computes the waveform of F_{pat_leak} from F_{vent} and F_{mask} monitoring and then of F_{resp} from Equation (8).

The MONITOR routine plots any combination of synchronized F_{vent} , F_{pat_leak} , F_{resp} , V_{Ti} , P_{ph} , and P_{es} signals within the selected time window, and also enables the calculation of the number of respiratory cycles. Statistical analysis, including mean, standard deviation, and standard error of the mean, has been applied to the total number of respiratory cycles for all the variables studied.

The TIME routine calculates the time of onset (T_{ins_O}) and end (T_{ins_E}) of inspiration and from them, the inspiratory time (T_{ins}), expiratory time (T_{exp}), and respiratory frequency (RR).

Once V_{Ti} signal has been calculated as the integration of F_{resp} over inspiratory time, the FLOW_VOLUME routine computes the total tidal volume (VT) as the difference between V_{Ti} at T_{ins_E} and V_{Ti} at T_{ins_O} . The FLOW_VOLUME routine also gives the peak inspiratory flow (PIF) as the maximum value of F_{resp} during inspiration, minute volume (MV) as the product between VT and RR, the ratio between VT and T_{ins} (VT/T_{ins}) or T_{exp} (VT/T_{exp}), and the ratio between RR and VT (RR/VT).

The PRESSURE routine implements the algorithm that defines the beginning of the inspiratory effort, i.e., beginning of negative P_{es} drop (T_{drop_0}), and computes the interval between T_{drop_0} and T_{ins_O} (i.e., T_{delay}). The PRESSURE routine also computes the intrinsic positive end expiratory pressure (PEEPi), total change in P_{es} across inspiration (ΔP_{esi}), transpulmonary pressure at end of inspiration (P_{tpei}), dynamic lung compliance (CL_{dyn}), and total lung resistance (RL_{tot}). PEEPi was determined as the difference between P_{es} at T_{drop_0} and P_{es} at T_{ins_O} , ΔP_{esi} as the difference between P_{es} at T_{ins_O} and P_{es} at T_{ins_E} , whereas P_{tpei} as P_{es} value at T_{ins_E} . CL_{dyn} was determined as the ratio of VT to ΔP_{esi} , while RL_{tot} as the mean difference between total and static P_{es} values divided by the mean F_{resp} , both evaluated considering T_{ins} interval. The inspiratory static P_{es} curve (P_{esst}) was extrapolated by dividing V_{Ti} by CL_{dyn} . In addition, the peak-to-peak variation in P_{es} swing (ΔP_{es_sw}) was calculated.

The CAMPBELL routine plots the inspiratory Campbell diagram with V_{Ti} on the Y axis and P_{es} on the X axis. The diagram shows the inspiratory P_{es} curve and the lines of P_{esst} , extrapolated line of chest wall static recoil pressure (P_{stcwr}), and P_{stcwr} increased by PEEPi value. P_{stcwr} has been extrapolated dividing V_{Ti} by the static compliance of the chest wall (CCW), which has been estimated as 4% of the theoretical inspiratory vital capacity divided by 1 cmH₂O.

From the Campbell diagram, the WORK routine computes the different components of inspiratory WOB, which are as follows:

- (1) Inspiratory resistive work (WOBres) is calculated as the area delimited by the P_{es} curve and the P_{esst} line;
- (2) Inspiratory elastic work related to lung expansion (WOBelas_lung) is calculated as the triangular area delimited by the P_{esst} lines and the horizontal line corresponding to the value that P_{es} assumes at T_{ins_O} ;

- (3) Inspiratory elastic work related to chest expansion ($WOB_{\text{Belas_chest}}$) is calculated as the triangular area delimited by the P_{stcwr} lines and the horizontal line corresponding to the value that P_{es} assumes at $T_{\text{ins_O}}$;
- (4) Additional elastic work done by the patient if $PEEP_i$ occurs (WOB_{PEEP_i}) is calculated as the area between the two P_{stcwr} lines spaced by $PEEP_i$.

The total elastic work ($WOB_{\text{Belas_tot}}$) was calculated as the sum of $WOB_{\text{Belas_lung}}$, $WOB_{\text{Belas_chest}}$, and WOB_{PEEP_i} . The total inspiratory WOB (WOB_{tot}) was computed as the sum of $WOB_{\text{Belas_tot}}$ and WOB_{res} components, while WOB_{tot} per minute ($WOB_{\text{tot_min}}$) and WOB_{tot} per liter ($WOB_{\text{tot_lit}}$) as the product of WOB_{tot} and RR and the ratio of WOB_{tot} to VT. The units employed for WOB were $\text{cmH}_2\text{O}\cdot\text{liters}$ or joule.

The PTP routine computes the different components of inspiratory PTP from P_{es} , P_{esst} and P_{stcwr} curves as follows:

- (1) Inspiratory resistive PTP (PTP_{res}) is calculated as the area delimited by the P_{es} and the P_{esst} curves;
- (2) Inspiratory elastic PTP related to lung expansion ($PTP_{\text{elas_lung}}$) is calculated as the area delimited by the P_{esst} curve and the horizontal line corresponding to the value that P_{es} assumes at $T_{\text{ins_O}}$;
- (3) Inspiratory elastic PTP related to chest expansion ($PTP_{\text{elas_chest}}$) is calculated as the area delimited by the P_{stcwr} curve and the horizontal line corresponding to the value that P_{es} assumes at $T_{\text{ins_O}}$;
- (4) The additional elastic PTP done by the patient if $PEEP_i$ occurs (PTP_{PEEP_i}) is calculated as the area between the two P_{stcwr} curves spaced by $PEEP_i$.

The total elastic PTP ($PTP_{\text{elas_tot}}$) was calculated as the sum of PTP_{PEEP_i} , $PTP_{\text{elas_lung}}$, and $PTP_{\text{elas_chest}}$. The total inspiratory PTP (PTP_{tot}) was computed as the sum of $PTP_{\text{elas_tot}}$ and PTP_{res} components, while PTP_{tot} per minute ($PTP_{\text{tot_min}}$) as the product of PTP_{tot} and RR. The units employed for PTP were $\text{cmH}_2\text{O}\cdot\text{s}$.

2.7.3. Mathematical Model

The mathematical model employed here is based on linear respiratory mechanics applied for determining the different components of resistance and compliance related to lung and chest expansion/recoil dynamics [14–16]. The model takes into account quasi-static variations of such respiratory parameters inside each single spontaneous breath. The effects of non-linearity on respiratory mechanics and, in particular, on WOB and PTP, had been evaluated and considered negligible [17].

2.8. Application of Pro_HFNC to Set HFNC Optimal Flow

The Pro_HFNC was clinically tested on five infants under six months of age who were treated with HFNC for mild to moderate respiratory distress. The clinical protocol is shown in Figure 4 in two flowcharts (blue and orange background). P_{es} measurement may or may not be included. Prior to commencing the HFNC, an esophageal catheter was inserted to measure P_{es} and a ventilatory mask connected to a PNT (PNT_2) was applied on the infant's face to measure PIF. The first 20 s of monitoring were discarded due to the potential effect on the flow signal of the trigeminal reflex elicited by the mask's contact with the face. When the flow signal was stable and the breathing was regular, we assumed that the PIF measurement was accurate. At this point, the HFNC flow rate was set 1 L/min higher than the infant's PIF. After HFNC was initiated, we measured the infant's PIF while the facial mask was applied to the infant's face without moving the nasal cannula. Once again, the first page was discarded, and the flow signal was recorded for 60 s (3 monitor pages). All signals were analyzed offline.

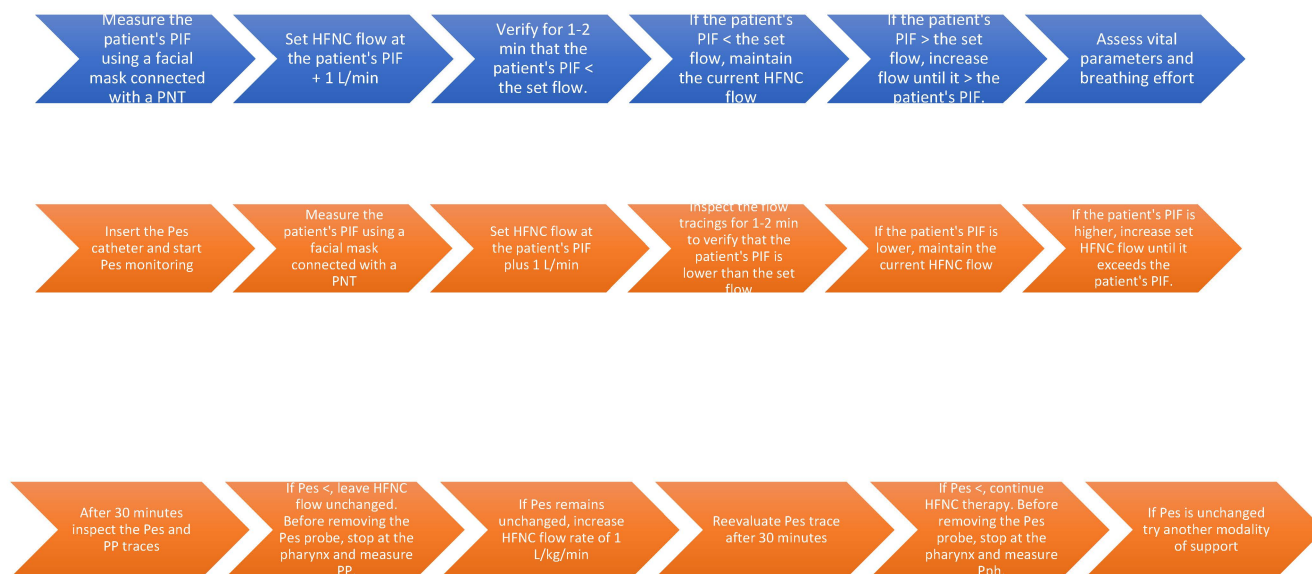


Figure 4. The flow chart in blue illustrates the protocol for using the monitoring system with only flow measurement, while the chart in orange displays the protocol based on both flow and pressure measurements.

3. Results

3.1. Optimal Flow Detection

In Figure 5a are shown F_{vent} (blue trace), F_{pat_leak} (green trace), and F_{resp} (red trace), as they appeared on the LAP's monitor when the Pro_HFNC was connected to a 2.3 kg infant with bronchiolitis treated with the HFNC set at 2 L/min. As expected, we found that the F_{vent} signal was not constant but sinusoidal in shape according to the patient's breathing effort. The sinusoidal shape of the F_{vent} signal makes it more difficult to understand which flow was set on the HFNC by the flow meter, and whether the resulting F_{vent} was high enough to meet the patient's flow demands. By turning the PS coupled with DFT on the position 2 (i.e., patient's disconnection from the VC, Figure 1) we found that F_{syst} value was slightly lower than the flow meter estimated value, confirming the inappropriateness of the flow meter to indicate exact F_{syst} value.

To verify on the LAP's monitor the condition of optimal flow rate in every instance of breath ($F_{vent} > F_{resp}$), while the patient was receiving the HFNC treatment, we looked at F_{vent} , F_{resp} , and F_{pat_leak} signals, following the subsequent reasoning: if F_{vent} is higher than F_{resp} at any time of inspiration, no air from the environment should be drawn into the OM. As a result, F_{pat_leak} signal should always be positive, i.e., no gas flow is entering the OM from the environment. Differently, if at any time F_{pat_leak} signal becomes negative during inspiration that will indicate that some air from the environment is entering the OM and, thus, the patient's airway. This condition is undesirable when using HFNC because it hampers its mechanisms of action. Thus, by observing the green line (F_{pat_leak} signal), it is possible to find the breaths in which the F_{pat_leak} troughs are below the zero line (Figure 5a). In this case, by increasing F_{syst} it will be possible to re-establish the condition by which F_{pat_leak} is always above the zero line (Figure 5b). Another way to look at the appropriateness of HFNC flow rate is based on the control of the blue trace (F_{vent}), i.e., whether it is above or below the red trace (F_{resp}). If HFNC is working properly, the peaks of the blue trace (F_{vent} signal) should always be above the peaks of the red trace (F_{resp} signal). In Figure 5a, it can be noted that the patient's breaths 1, 3, 6, 7, 9, 10, 11, and 12 did not meet the requirements for the appropriateness of F_{syst} (F_{pat_leak} below the zero line), while, in Figure 5b, increasing F_{syst} from 2 to 3 L/min, F_{pat_leak} troughs became always positive and, accordingly, the peaks of F_{vent} (blue trace) were always higher than those of F_{resp} (red trace). Finally, in Figure 6a, where F_{vent} does not meet F_{resp} ($F_{syst} = 2$ L/min), it can be noted that the P_{ph} troughs were

always below the zero line, whereas in Figure 6b, where F_{vent} is always higher than F_{resp} ($F_{syst} = 3 \text{ L/min}$), all troughs of Pph trace were positive.

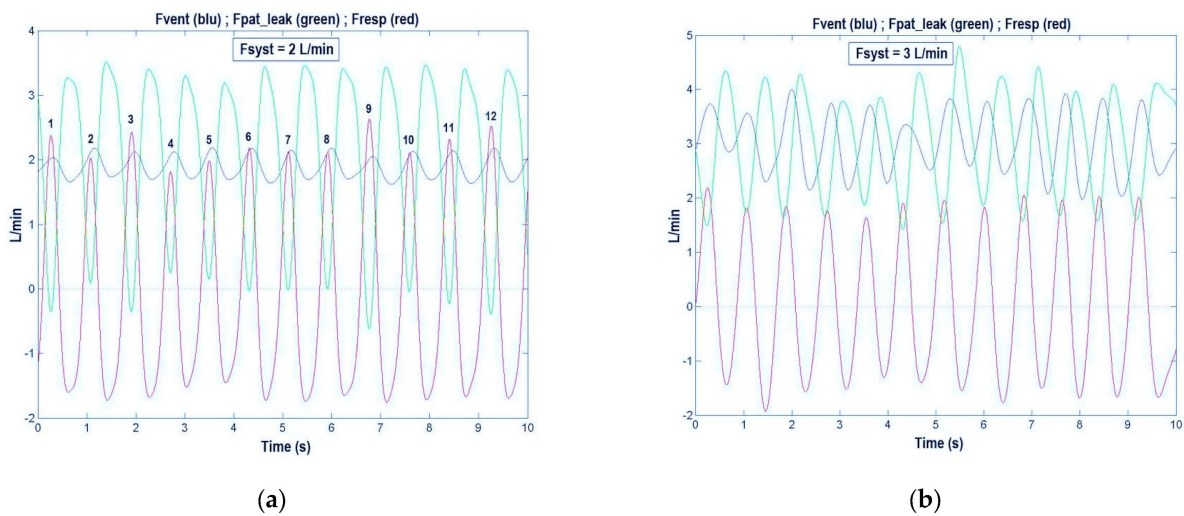


Figure 5. The blue trace shows the high-flow nasal cannula (HFNC) flow delivered to the patient (F_{vent}) and the green trace shows the total flow leak from patient (F_{pat_leak}), which represents the difference between F_{vent} and the respiratory flow (F_{resp} , red trace). The three traces permit us to verify if the F_{vent} meets the patient’s inspiratory flow demands, i.e., if the condition $F_{vent} > F_{resp}$ is always true or, alternatively, if the condition $F_{pat_leak} > 0$ is always true. (a) $F_{syst} = 2 \text{ L/min}$: F_{vent} is insufficient in several breaths: 1, 3, 6, 7, 9, 10, 11, and 12. (b) $F_{syst} = 3 \text{ L/min}$: F_{vent} always meets the patient’s flow demands (F_{vent} is always higher than F_{resp}) (see Section 3.1).

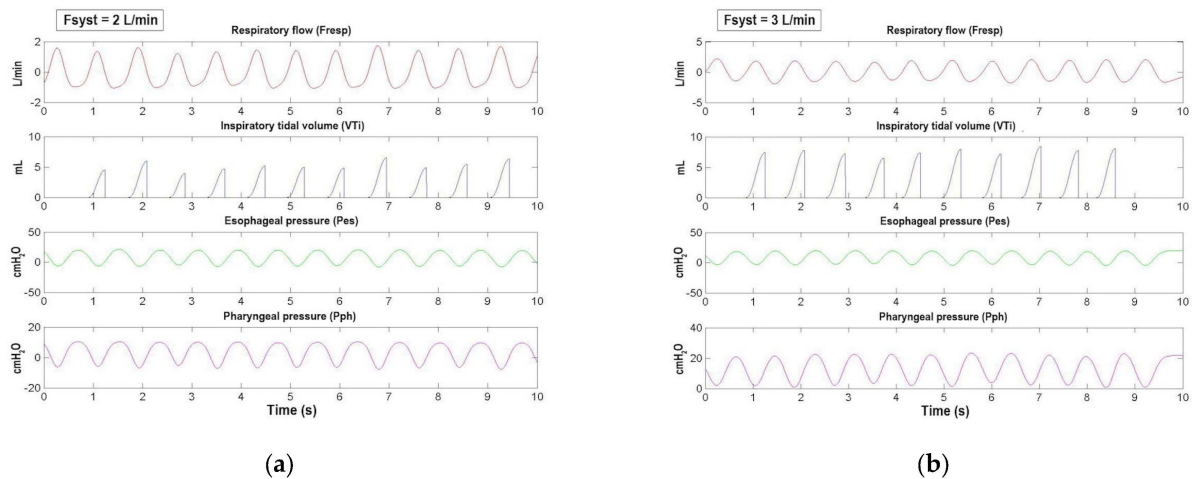


Figure 6. From top to bottom are shown the synchronized signals of respiratory flow (F_{resp} , red trace), inspiratory tidal volume (V_{Ti} , dark gray trace), esophageal pressure (P_{es} , green trace), and pharyngeal pressure (P_{ph} , magenta trace) of a representative infant as a function of time. (a) As we showed in Figure 5a by using F_{vent} , F_{pat_leak} , and F_{resp} signals, in this figure ($F_{syst} = 2 \text{ L/min}$) we confirmed how F_{vent} was insufficient to meet F_{resp} by using the P_{ph} signal, whose troughs are always negative. (b) Differently from (a), in this figure ($F_{syst} = 3 \text{ L/min}$), F_{vent} is increased to meet F_{resp} . This condition is confirmed by the troughs of the pharyngeal pressure, which are always positive (see Section 3.1). From these signals it was possible to calculate the most significant parameters of the patient’s respiratory profile (see Section 3.2).

To calculate the amount of volume drawn from the environment into OM (i.e., when F_{vent} is lower than F_{resp} and F_{pat_leak} is negative) we calculated the area (integral over

time) of the green curve (Fpat_leak) part below the zero line and subtracted this value from the area of the red curve (Fresp) (Figure 5a).

3.2. Respiratory Profile Evaluation

To calculate any parameter relative to patient’s respiratory profile, we needed first to detect for every breath Tins_O and Tins_E, i.e., the timing of inspiration. The timing of inspiration is crucial for the identification of the onset and the end of inspiration on the Pes and Pph signals. We accomplished this task by looking at the Fresp signal: whenever Fresp crossed the zero line, we were in the presence of either Tins_O or Tins_E. The MATLAB TIME routine was used to differentiate Tins_O from Tins_E. Specifically, if the TIME routine finds a Fresp value corresponding to zero, it checks the algebraic sign of the next value. If the next value is positive then we are in the presence of Tins_O, if negative of Tins_E. Then, by integrating over time the inspiratory tract of the F_resp waveform, we obtain the VTi signal, and therefore VT, as the difference between VTi at Tins_E and VTi at Tins_O. Afterwards, by synchronizing the waveforms of Fresp, VTi, Pes, and Pph (Figure 6a,b shows the signals of a representative infant treated with HFNC therapy), it is possible to calculate the most significant parameters of patient’s respiratory profile (Table 1).

Table 1. Most significant parameters of patient’s respiratory profile evaluated by Pro_HFNC ¹.

Parameters [Units]	Signals Required	Parameters Required
Tins_O [s]	Fresp	
Tins_E [s]	Fresp	
Tins [s]		Tins_O; Tins_E
Texp [s]		Tins_E; Tins_O
Tins/Texp		Tins; Texp
RR [act/min]		Tins; Texp
VT [mL]	VTi	Tins_O; Tins_E
VM [mL/min]		VT; RR
VT/Tins [mL/s]		VT; Tins
VT/Texp [mL/s]		VT; Texp
RR/VT [act/min/mL]		RR; VT
PIF [L/min]	Fresp	
Tdrop_0 [s]	Pes	
Tdelay [s]		Tdrop_0; Tins_O
PEEPi [cmH ₂ O]	Pes	Tdrop_0; Tins_O
ΔPesi [cmH ₂ O]	Pes	Tins_O; Tins_E
ΔPes_sw [cmH ₂ O]	Pes	Tdrop_0
Ptpei [cmH ₂ O]	Pes	Tins_E
CLdyn [mL/cmH ₂ O]		VT; ΔPesi
RLtot [cmH ₂ O/mL/s]	Pes; VTi; Fresp	Tins_O; Tins_E; CLdyn; VT
PTPres [cmH ₂ O·s]	Pes; VTi	Tins_O; Tins_E; CLdyn
PTPelas_lung [cmH ₂ O·s]	VTi	Tins_O; Tins_E; CLdyn
PTPelas_chest [cmH ₂ O·s]	VTi	Tins_O; Tins_E; CLdyn
PTPelas_PEEPi [cmH ₂ O·s]	VTi	Tins_O; Tins_E; CLdyn; PEEPi
PTPelas_tot [cmH ₂ O·s]		PTP_PEEPi; PTPelast_lung; PTPelast_chest
PTPtot [cmH ₂ O·s]		PTPelas_tot; PTPres
PTPtot_min [cmH ₂ O·s/min]		PTPtot; RR
WOBres [cmH ₂ O·mL]; [joule]	Pes; VTi	Tins_O; Tins_E; CLdyn
WOBelas_lung [cmH ₂ O·mL]; [joule]	VTi	Tins_O; Tins_E; CLdyn
WOBelas_chest [cmH ₂ O·mL]; [joule]	VTi	Tins_O; Tins_E; CLdyn
WOB_PEEPi [cmH ₂ O·mL]; [joule]	VTi	Tins_O; Tins_E; CLdyn; PEEPi
WOBelas_tot [cmH ₂ O·mL]; [joule]		WOB_PEEPi; WOBelas_lung; WOBelas_chest
WOBtot [cmH ₂ O·mL]; [joule]		WOBelas_tot; WOBres
WOBtot_min [cmH ₂ O·mL/min]; [joule/min]		WOBtot; RR
WOBtot_lit [cmH ₂ O·mL/L]; [joule/L]		WOBtot; VT

¹ See Section 2.7.2.

To calculate all the parameters listed in Table 1, we have recorded Pes curve synchronized with the Fresp signal.

Figure 7 shows how PEEPi, Δ Pesi, Δ Pes_sw and Ptpci were determined on a Pes swing of a representative patient. Figure 8 shows the different areas corresponding to the different inspiratory PTP components and how they were computed (see Section 2.7.2).

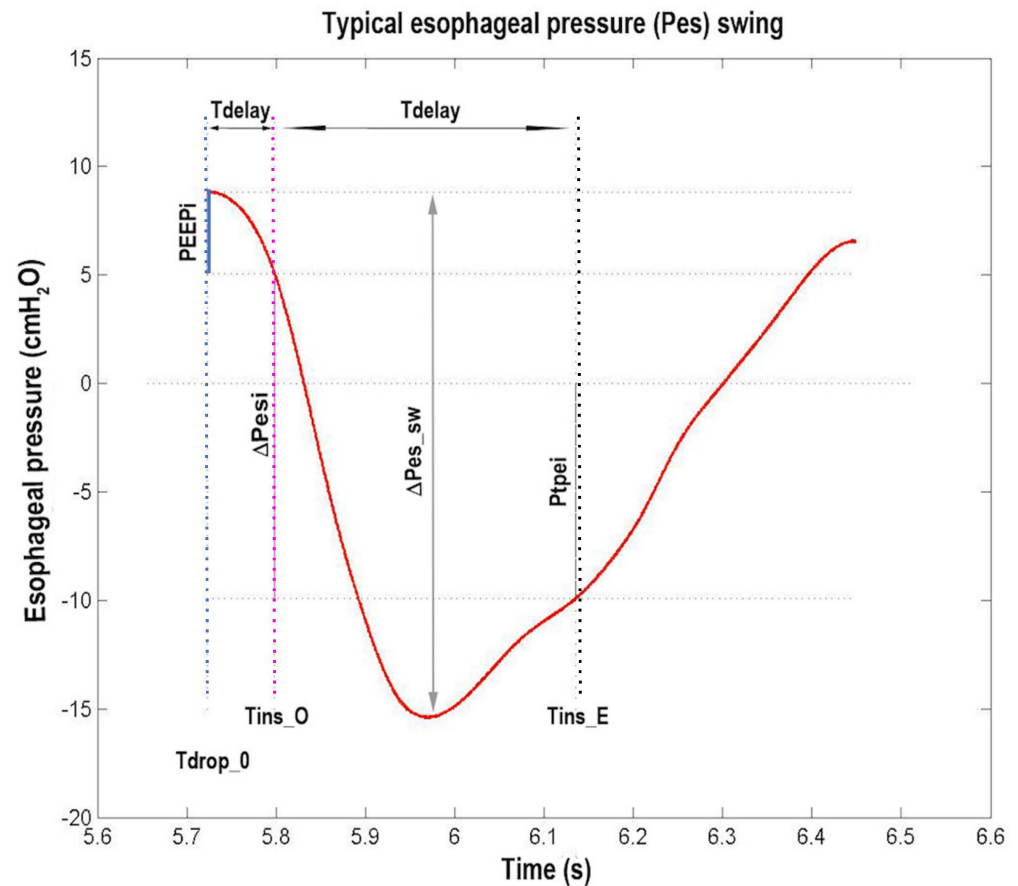


Figure 7. Typical esophageal pressure (Pes) swing (red trace) of a representative patient as a function of time. The dotted vertical lines are drawn (from left to right) at the beginning of inspiratory effort (Tdrop_0, blue line), at the beginning of inspiration (Tins_O, magenta line), and at the end of inspiration (Tins_E, black line), respectively. The dotted horizontal lines are drawn (from top to bottom) in correspondence to the Pes value at Tdrop_0, at Tins_O, at zero pressure, and at Tins_E. The size of the three continuous vertical segments (from left to right) defines the values of intrinsic positive end expiratory pressure (PEEPi, blue segment), total inspiratory Pes variation (Δ Pesi, magenta segment), and transpulmonary pressure at end of inspiration (Ptpci, black segment). The size of the continuous vertical double arrow defines the value of peak-to-peak Pes variation (Δ Pes_sw). From left to right, the size of the two continuous horizontal double arrows defines the value of the interval between Tdrop_0 and Tins_O (Tdelay) and of the inspiratory time (Tins), respectively (see Sections 2.7.2 and 3.2 and Table 1).

Finally, Figure 9 shows the curve and lines (CLdyn, CCW) composing Campbell's diagram, while Figure 10, the different areas corresponding to the different inspiratory WOB components and how they were computed (see Section 2.7.2).

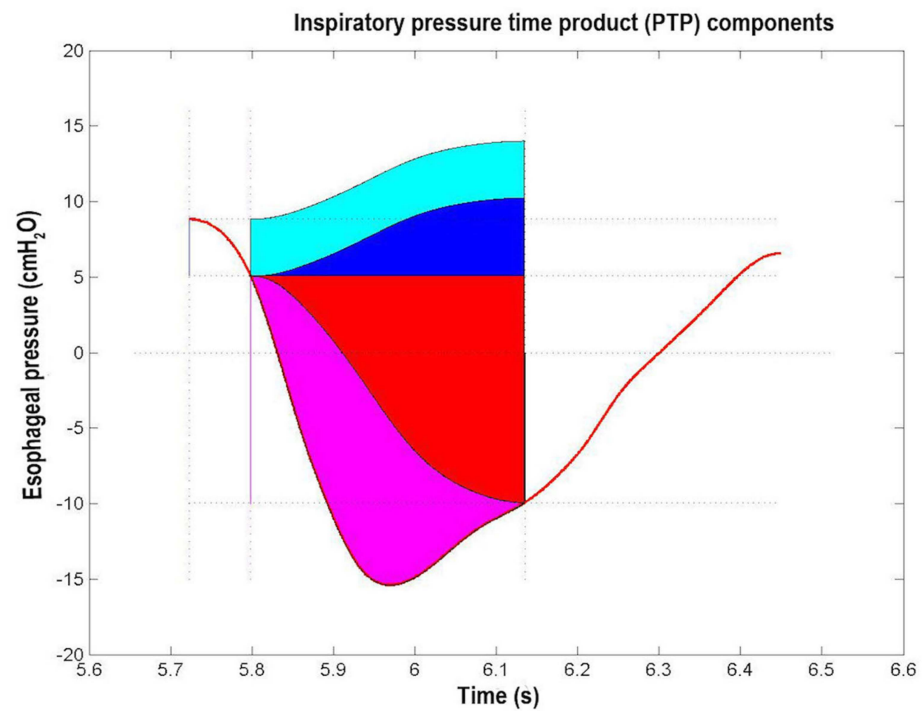


Figure 8. Inspiratory Pressure Time Product (PTP) of a typical esophageal pressure (Pes) swing (red trace) of a representative patient. The blu segment indicates intrinsic positive end expiratory pressure (PEEPi) value, the magenta segment indicates change in Pes value during inspiration, the black segment indicates the Pes value at the end of inspiration. The areas correspond to the various PTP components, i.e., PEEPi, PTP (PTP_PEEPi, cyan area), chest wall elastic PTP (PTPelast_chest, blue area), lung elastic PTP (PTPelast_lung, red area), and resistive PTP (PTPres, magenta area) (see Sections 2.7.2 and 3.2 and Table 1).

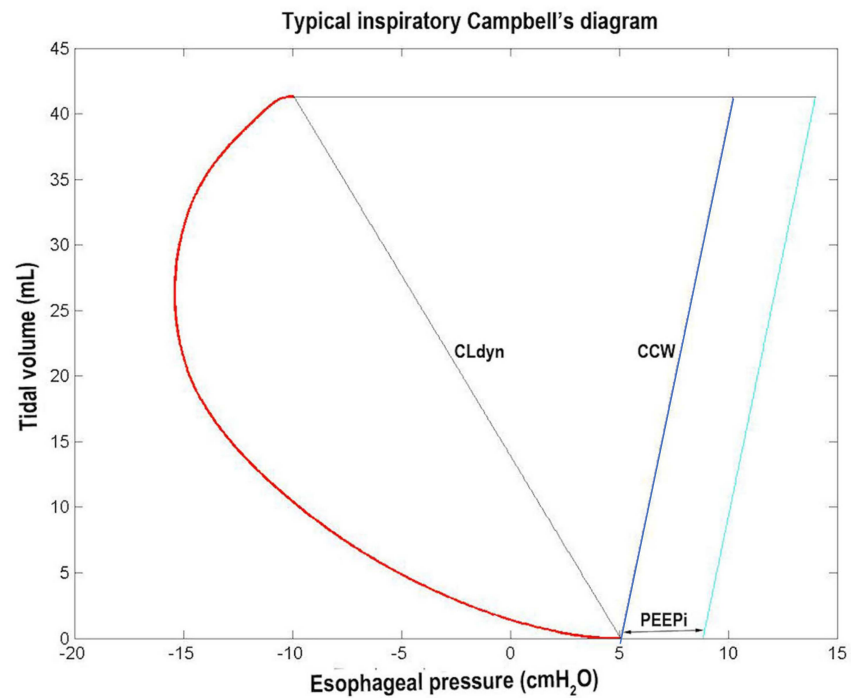


Figure 9. Typical inspiratory Campbell's diagram. The red curve represents the esophageal pressure (Pes) swing, while the black, blue, and cyan lines represent the variations during inspiration of the static Pes (Pest), the extrapolated chest wall static recoil pressure (Pstcwr), and the Pstcwr increased by PEEPi value, respectively (see Sections 2.7.2 and 3.2 and Table 1).

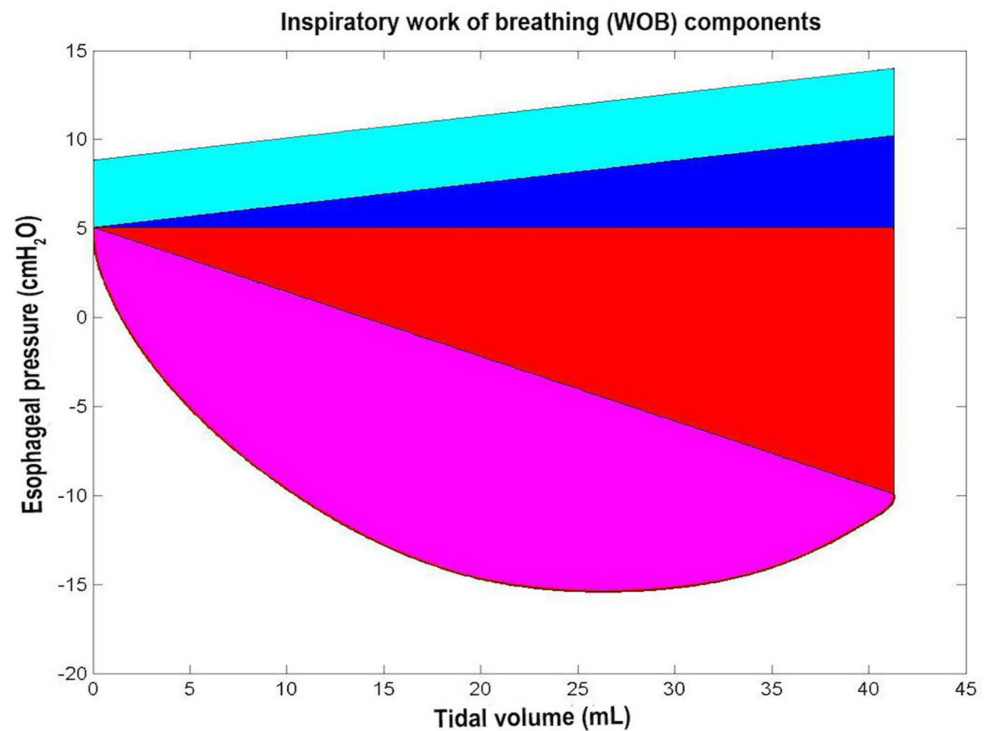


Figure 10. Inspiratory work of breathing (WOB). The cyan, blue, red, and magenta areas correspond to the following four WOB components: the intrinsic positive end expiratory pressure (PEEPi) WOB (WOB_PEEPi, cyan area), chest wall elastic WOB (WOBelas_chest, blue area), lung elastic WOB (WOBelas_lung, red area), and resistive WOB (WOBres, magenta area) (see Sections 2.7.2 and 3.2 and Table 1).

Table 2 shows the application of the clinical protocol as presented in the second flow chart. The difference between the empirical flow and the PIF-based flow is evident, as well as the impact on Pes. If the non-invasive flow chart were used, tidal volume data could be obtained instead of Pes, providing information on the efficacy of ventilation.

Table 2. Effects of high-flow nasal cannula (HFNC) flow settings (Fven) based on the patient’s body weight (Fven_kg) or patient’s peak inspiratory flow (Fven_PIF) on changes in esophageal pressure swing (Δ Pes_sw) and PIF.

Pt	Weight kg	Spontaneous Breathing				HFNC Therapy					
		Fven L/min	PIF L/min	Δ Pes_sw cmH ₂ O	Fven_kg L/min	Fven_PIF L/min	Δ Pes_sw_ HFNC_kg cmH ₂ O	Δ Pes_sw_ HFNC_PIF cmH ₂ O	PIF_ HFNC_kg L/min	PIF_ HFNC_PIF cmH ₂ O	
1	5.270	0	8.3	24	6	9	23	16	6.3	4.7	
2	3.450	0	4.8	18	4.5	6	15	12	3.9	3.2	
3	4.200	0	3.8	13	5	5	9	10	3.5	3.7	
4	4.930	0	5.8	18	6	7	15	13	5.0	4.5	
5	7.150	0	9.0	25	8	10	21	18	8.0	7.2	

Pt: patient.

Using the system as in the second flow chart of Figure 4 with the associated use of Pph catheter, Figure 11 shows the tracings of the Pph and Pes of an infant with mild respiratory distress during spontaneous breathing in oxygen, on HFNC at 4 L/min (1 L/kg/min) and on HFNC at 8 L/min (2 L/kg/min). In this infant, Pph oscillates from -10 cmH₂O to $+4$ cmH₂O during spontaneous breathing (mean value -3 cmH₂O), from -1 cmH₂O to $+7$ cmH₂O during HFNC at 4 L/min (mean value $+3$ cmH₂O), and from $+5$ cmH₂O to $+11$ cmH₂O at 8 L/min (mean value $+8$ cmH₂O). The Pes oscillates from -10 cmH₂O to

+10 cmH₂O during spontaneous breathing and from −1 cmH₂O to +8 cmH₂O at 4 L/min. With respect to the lower flow rate of 4 L/min, the higher flow rate of 8 L/min, while increasing the mean Pph value (+8 cmH₂O instead of +4 cmH₂O), did not have any further effect on Pes swings (from −1 cmH₂O to +8 cmH₂O), indicating that there was no further effect of flow on the respiratory effort.

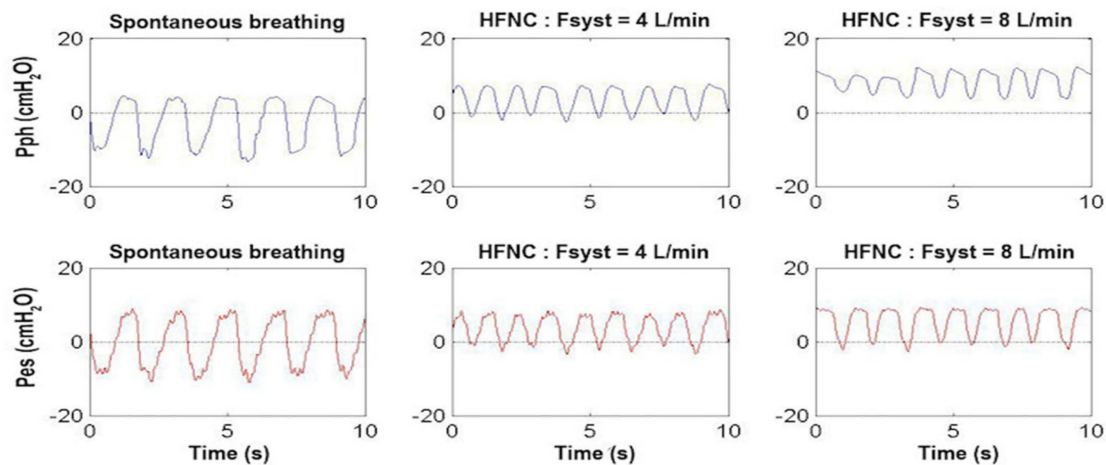


Figure 11. Pharyngeal pressure (Pph, **upper panels**, blue traces) and esophageal pressure (Pes, **lower panels**, red traces) waveform as a function of time in a representative patient weighing 4 kg with mild respiratory distress during spontaneous breathing (**left panels**), on high-flow nasal cannula (HFNC) with F_{syst} at 4 L/min (**middle panels**) and at 8 L/min (**right panels**). Note that the Pes swings were quite similar between HFNC 4 and 8 L/min indicating that there was no further effect of flow on the respiratory effort (see Section 3.2).

4. Discussion

HFNC is commonly used to treat mild to moderate respiratory distress in patients of different ages. This technique is based on the assumption that a warmed, humidified air/oxygen mixture, delivered through NC at a flow exceeding the patient's PIF, meets entirely the patient's flow demand and ensures no entrapment of air from the environment. As a result, the FiO₂ set on the HFNC equals the patient's FiO₂. In addition, the excess of the flow delivered by the HFNC continuously purges the nasopharyngeal dead space, thus eliminating dead space CO₂ and improving ventilation [1]. The high flow delivery by the HFNC also generates clinically significant intrapharyngeal pressure without the complications associated with traditional NCPAP (e.g., septal erosion, difficulties of maintaining device position, and discomfort). Nevertheless, the flow needed to generate significant and sufficient CPAP is presently unknown, which is why the use of HFNC as a replacement for CPAP is not without controversy [1,18]. The absence of a monitoring device makes HFNC flow optimization empirical. In adults, several researchers have attempted to optimize HFNC flow by measuring the patient's PIF through spirometry before commencing HFNC treatment. However, as we have shown, the patient's PIF can change after HFNC therapy, making these measurements unhelpful during treatment.

In this paper, we showed a simple way to set the optimal flow rate in infants receiving HFNC treatment based on the detection of several flow signals either from the HFNC (i.e., F_{syst} and F_{vent}), or from the patient (i.e., F_{mask}). This method is quick and easy to use because it is based on the insertion in a commercially available HFNC of a DFT (to detect F_{syst}) and two PNTs coupled with two DPTs (to detect F_{vent} and F_{mask}). The interface between the Pro_HFNC device and the patient is an OM which is applied during the procedures of PIF measurements, on the patient's face, and during HFNC treatment over the mouth and NC. Because this system requires a mask to be placed on the infant's face, it is difficult to use for continuous monitoring, either because of the infant's distress caused by the mask over time or because of the operator's need to maintain the mask

on the infant's face, which is not practical in the clinical setting for long periods of time. Although in this study we tested the use of our monitoring system in a small group of infants, there is no reason why it cannot be tested in older age groups. With children, a HFNC monitoring system which can measure P_{ph} is more important than with adults. One significant difference between infants and adults is the way they position their mouth during respiratory distress, especially when receiving mild sedation. Infants usually keep their mouths closed with their tongue attached to the palate. This may increase the risk of pulmonary overdistension because of increased P_{ph} with increasing inspiratory flow. In adults, the mouth is usually slightly open, which reduces P_{ph} and increases the safety of high flow rates.

The application of Pro_HFNC on a few infants demonstrated that F_{syst} set either by Sreenan formula ($\text{Flow (L/min)} = 0.92 + 0.68 \times \text{weight in kg}$) [18], or empirically based on the values suggested by the manufacturer ($1 \text{ L/kg/min} + 1$) does not always satisfy the patient's needs. In fact, we have shown in Figure 5a how in several breaths F_{vent} did not meet the patient's flow demand (F_{resp}). Although there are no guidelines on the use of HFNC in the adult or pediatric population, it is suggested to increase flow rate when the clinical condition of a patient treated with HFNC is not improving before other actions are implemented. Despite the fact that this approach often gives satisfying clinical results, we believe that having an objective device to set the optimal flow rate would make the physician's decision making easier and would allow for less complications arising from excessive flow delivery, such as lung hyperinflation, PEEP_i, and increased WOB.

In addition to optimal flow setting, another measure that guides the ventilatory treatment is the patient's respiratory profile characterization. This is easy to accomplish when the patient is on invasive ventilation because there is no gas leakage. Obviously, the evaluation of respiratory profile is not as easy in patients on non-invasive respiratory support because of the gas leakages from around the interface. Several methods have been developed to obtain objective indexes of respiratory mechanics in patients undergoing non-invasive ventilation. A number of techniques are now available, such as electric impedance plethysmography (EIP), respiratory inductive plethysmography (RIP), magnetometers/strain gauge sensors, and piezoresistive materials displacement sensor. Compared with other techniques, RIP has the advantages of greater accuracy, better sensitivity, and higher safety for patients, and has been used widely in clinical and research settings. However, even if RIP is considered reliable for determining lung volume changes and thoraco-abdominal asynchrony indexes, the accuracy of the calibration coefficients require the HFNC suspension with the consequence of losing the benefits of this treatment. In addition, the asynchrony indexes, which are the most important respiratory mechanical parameters obtained using RIP, are merely nonspecific indicators of abnormal breathing. The real-time implementation of flow-leak algorithm [13] offered by the functional features of Pro_HFNC, in addition to optimal flow detection and HFNC setting, allows the simultaneous monitoring of F_{resp}, V_{Ti}, P_{es}, and P_P signals and therefore also the determination of the most relevant parameters of patient's respiratory profile (Table 1) without suspending HFNC treatment. To the best of our knowledge, this is the first study that measures all these variables in patients treated with HFNC. At any age, respiratory distress can be associated with some degree of bronchial obstruction because of bronchial secretions or edema of the bronchial wall, which can lead in association with the high respiratory rate to increased breathing effort secondary to dynamic hyperinflation and PEEP_i [19]. Therefore, part of the supportive effect of non-invasive respiratory assistance helps relieving the effort to overcome PEEP_i. To set the adequate HFNC flow rate, which determines a P_{ph} level required to overcome PEEP_i, it is therefore paramount for those who work in intensive care units or in respiratory units to monitor in real time the patient's respiratory profile. In this study we were able to measure PEEP_i as well as the relevant measures of respiratory effort including the inspiratory resistive PTP (PTP_{res}), PTP_{elas_lung}, PTP_{elas_chest}, PTP_{PEEPi}, and PTP_{tot}. We also calculated the WOB_{res}, WOB_{elas_lung}, WOB_{elas_chest}, WOB_{PEEPi}, and WOB_{tot}. Although these parameters are useful for adjusting flow settings, they require

the insertion of an esophageal catheter, making this system more invasive and difficult to use. It is likely that the parameters requiring pressure measurements will be used for research purposes or in highly trained clinical centers.

Another interesting clinical point we made in our study comes from the unexpected effect of increasing flow rate on effort of breathing (Figure 11). While 1 L/kg/min reduced Pes swings in an infant with mild respiratory distress, higher flow rate (2 L/kg/min) did not further decrease breathing effort. Instead, it increased P_{ph} mean values, potentially causing a detrimental effect on the patient by increasing pulmonary air trapping. These data further highlight the need for a bedside tool to monitor lung mechanics in infants treated with HFNC.

A strength of the system is that during flow optimization, the system is completely non-invasive and the mask on the infant's face does not interfere with HFNC treatment. Unlike spirometry, it does not add dead space. This monitoring system enables real-time visualization of the HFNC and patient flow and volume traces, allowing for adjustments to the delivered flow rate and immediate re-evaluation. In the non-invasive version, the only disposable part is the ventilation mask, whereas the pneumotachographs are reusable after disinfection.

Our system has limitations. Firstly, monitoring can only occur for specific periods of time and not continuously. Secondly, the system was only tested on infants, so it is uncertain whether it would be as useful in an adult population as it is in young infants.

5. Conclusions

In conclusion, in this paper we have shown a new system (Pro_HFNC) that permits us to set in real time the optimal flow rate and to evaluate respiratory profile in patients with respiratory distress treated with HFNC. With Pro_HFNC, the determination of optimal flow rate is simple to perform, it does not necessitate particular skills, and, most importantly, it does not require HFNC interruption. Pro_HFNC also allows for F_{syst} control during treatment. Finally, if connected to P_{ph} and Pes catheters, Pro_HFNC allows for the calculation of numerous parameters of patient's respiratory profile that may be useful to continue or interrupt HFNC treatment.

We believe that for a better control of respiratory parameters, the application of HFNC combined with the Pro_HFNC will grow further and with it the opportunities it offers.

Author Contributions: Conceptualization, F.M. and P.P.; methodology, F.M. and P.P.; software, F.M.; validation, F.M. and P.P.; formal analysis, F.M. and P.P.; investigation, F.M. and P.P.; data curation, F.M. and P.P.; writing—original draft preparation, F.M. and P.P.; writing—review and editing, F.M. and P.P.; visualization, F.M. and P.P.; supervision, F.M. and P.P. All authors have read and agreed to the published version of the manuscript.

Funding: This research received no external funding.

Institutional Review Board Statement: The study was conducted in accordance with the Declaration of Helsinki, and approved by the Ethics Committee of Policlinico Umberto I of Rome, Italy, (protocol code 3471 and 11/23/16).

Informed Consent Statement: Informed consent was obtained from all infants' parents involved in the study.

Data Availability Statement: Data are contained within the article. Further data that support the findings of this study are available upon request from the corresponding author. The data are not publicly available due to privacy or ethical restrictions.

Conflicts of Interest: The authors declare no conflicts of interest.

References

1. Dysart, K.; Miller, T.L.; Wolfson, M.R.; Shaffer, T.H. Research in high flow therapy: Mechanisms of action. *Respir. Med.* **2009**, *103*, 1400–1405. [[CrossRef](#)] [[PubMed](#)]
2. Lee, J.H.; Rehder, K.J.; Williford, L.; Cheifetz, I.M.; Turner, D.A. Use of high flow nasal cannula in critically ill infants, children, and adults: A critical review of the literature. *Intensive Care Med.* **2013**, *39*, 247–257. [[CrossRef](#)] [[PubMed](#)]
3. Rubin, S.; Ghuman, A.; Deakers, T.; Khemani, R.; Ross, P.; Newth, C.J. Effort of breathing in children receiving high-flow nasal cannula. *Pediatr. Crit. Care Med.* **2014**, *15*, 1–6. [[CrossRef](#)]
4. Papoff, P.; Caresta, E.; Luciani, S.; Pierangeli, A.; Scagnolari, C.; Giannini, L.; Midulla, F.; Montecchia, F. The starting rate for high-flow nasal cannula oxygen therapy in infants with bronchiolitis: Is clinical judgment enough? *Pediatr. Pulmonol.* **2021**, *56*, 2611–2620. [[CrossRef](#)] [[PubMed](#)]
5. Hasan, R.A.; Habib, R.H. Effects of flow rate and airleak at the nares and mouth opening on positive distending pressure delivery using commercially available high-flow nasal cannula systems: A lung model study. *Pediatr. Crit. Care Med.* **2011**, *12*, e29–e33. [[CrossRef](#)]
6. Milési, C.; Requirand, A.; Douillard, A.; Baleine, J.; Nogué, E.; Matecki, S.; Amedro, P.; Pons-Odena, M.; Cambonie, G. Assessment of Peak Inspiratory Flow in Young Infants with Acute Viral Bronchiolitis: Physiological Basis for Initial Flow Setting in Patients Supported with High-Flow Nasal Cannula. *J. Pediatr.* **2021**, *231*, 239–245.e1. [[CrossRef](#)] [[PubMed](#)]
7. Li, J.; Deng, N.; He, W.J.A.; Yang, C.; Liu, P.; Albuainain, F.A.; Ring, B.J.; Miller, A.G.; Rotta, A.T.; Guglielmo, R.D.; et al. The effects of flow settings during high-flow nasal cannula oxygen therapy for neonates and young children. *Eur. Respir. Rev.* **2024**, *33*, 230223. [[CrossRef](#)] [[PubMed](#)]
8. Armarego, M.; Forde, H.; Wills, K.; Beggs, S.A. High-flow nasal cannula therapy for infants with bronchiolitis. *Cochrane Database Syst. Rev.* **2024**, *3*, CD009609. [[CrossRef](#)] [[PubMed](#)]
9. Nielsen, K.R.; Ellington, L.E.; Gray, A.J.; Stanberry, L.I.; Smith, L.S.; DiBlasi, R.M. Effect of High-Flow Nasal Cannula on Expiratory Pressure and Ventilation in Infant, Pediatric, and Adult Models. *Respir. Care* **2018**, *63*, 147–157. [[CrossRef](#)] [[PubMed](#)]
10. Gray, A.J.; Nielsen, K.R.; Ellington, L.E.; Earley, M.; Johnson, K.; Smith, L.S.; DiBlasi, R.M. Tracheal pressure generated by high-flow nasal cannula in 3D-Printed pediatric airway models. *Int. J. Pediatr. Otorhinolaryngol.* **2021**, *145*, 110719. [[CrossRef](#)] [[PubMed](#)]
11. Montecchia, F.; Luciani, S.; Cicchetti, R.; Grossi, R.; Midulla, F.; Moretti, C.; Papoff, P. Pharyngeal and esophageal pressure measurements to evaluate respiratory mechanics in infants on high flow nasal cannula: A feasibility study. In Proceedings of the IEEE International Symposium on Medical Measurements and Applications (MeMeA), Turin, Italy, 7–9 May 2015; pp. 234–239. [[CrossRef](#)]
12. Simbruner, G.; Coradello, H.; Lubec, G.; Pollak, A.; Salzer, H. Respiratory compliance of newborns after birth and its prognostic value for the course and outcome of respiratory disease. *Respiration* **1982**, *43*, 414–423. [[CrossRef](#)] [[PubMed](#)]
13. Montecchia, F.; Midulla, F.; Papoff, P. A flow-leak correction algorithm for pneumotachographic work-of-breathing measurement during high-flow nasal cannula oxygen therapy. *Med. Eng. Phys.* **2018**, *54*, 32–43. [[CrossRef](#)] [[PubMed](#)]
14. Mayaud, L.; Lejaille, M.; Prigent, H.; Louis, B.; Fauroux, B.; Lofaso, F. An open-source software for automatic calculation of respiratory parameters based on esophageal pressure. *Respir. Physiol. Neurobiol.* **2014**, *192*, 1–6. [[CrossRef](#)] [[PubMed](#)]
15. Koumoundouros, E.; Santamaria, J.; Patterson, J. The comparison of work of breathing methodologies on a patient model. In Proceedings of the International Conference of the IEEE Engineering in Medicine and Biology Society (EMBS), Istanbul, Turkey, 25–28 October 2001. [[CrossRef](#)]
16. Silberberg, A.R.; Sanberg, K. Direct measurements of airways pressure in ventilated very low birth weight infants. In Proceedings of the International Conference of the IEEE Engineering in Medicine and Biology Society (EMBS), New York, NY, USA, 30 August–3 September 2006; pp. 2868–2870. [[CrossRef](#)]
17. Athanasiades, A.; Ghorbel, F.; Clark, J.W.; Niranjana, S.C.; Liu, C.H.; Zwischenberger, J.B.; Bidani, A. The work of breathing in nonlinear model of respiratory mechanics. In Proceedings of the International Conference of the IEEE Engineering in Medicine and Biology Society (EMBS), Chicago, IL, USA, 30 October–2 November 1997; pp. 2161–2164.
18. Sreenan, C.; Lemke, R.P.; Hudson-Mason, A.; Osiovič, H. High-flow nasal cannulae in the management of apnea of prematurity: A comparison with conventional nasal continuous positive airway pressure. *Pediatrics* **2001**, *107*, 1081–1083. [[CrossRef](#)] [[PubMed](#)]
19. Pepe, P.E.; Marini, J.J. Occult positive end-expiratory pressure in mechanically ventilated patients with airflow obstruction: The auto-PEEP effect. *Am. Rev. Respir. Dis.* **1982**, *126*, 166–170. [[CrossRef](#)] [[PubMed](#)]

Disclaimer/Publisher’s Note: The statements, opinions and data contained in all publications are solely those of the individual author(s) and contributor(s) and not of MDPI and/or the editor(s). MDPI and/or the editor(s) disclaim responsibility for any injury to people or property resulting from any ideas, methods, instructions or products referred to in the content.